NASA TECHNICAL NOTE

NASA TN D-4556

SUPPRESSION OF TEMPERATURE RISE IN LOSSY DIODES INSIDE RESONANT CAVITIES BY APPLICATION OF PRESSURIZED LIQUID NITROGEN

by Hans-Juergen C. Blume

Langley Research Center
Langley Station, Hampton, Va.

NATIONAL AERONAUTICS AND SPACE ADMINISTRATION • WASHINGTON, D. C. • MAY 1968

SUPPRESSION OF TEMPERATURE RISE IN LOSSY DIODES INSIDE RESONANT CAVITIES BY APPLICATION OF PRESSURIZED LIQUID NITROGEN

By Hans-Juergen C. Blume

Langley Research Center
Langley Station, Hampton, Va.

NATIONAL AERONAUTICS AND SPACE ADMINISTRATION

For sale by the Clearinghouse for Federal Scientific and Technical Information
Springfield, Virginia 22151 – CFSTI price $3.00

SUPPRESSION OF TEMPERATURE RISE IN LOSSY DIODES INSIDE RESONANT CAVITIES BY APPLICATION OF PRESSURIZED LIQUID NITROGEN

By Hans-Juergen C. Blume
Langley Research Center

SUMMARY

The suppression of temperature rise in lossy diodes due to electrical power dissipation inside resonant cavities of low-noise devices such as parametric amplifiers is essential in maintaining optimum low-noise performance. This suppression can be achieved by the application of pressurized liquid nitrogen inside the cavity. The expected temperature of the lossy diode under this condition is estimated by (a) a calculation based on the heat-flow equations and (b) a salt-solution test. The results are correlated with direct measurements which reveal a temperature rise of 3.3° K above the temperature of liquid nitrogen at 1 atmosphere. The resonant-frequency shift due to the liquid-nitrogen dielectric is estimated and its correlation with measurements is included. The results indicate that this type of cooling can be successfully used and is particularly effective for parametric amplifiers with medium-quality varactor diodes.

INTRODUCTION

The demand for ultra-low-noise preamplification, especially in long-range telemeter and radar systems, has stimulated the development of devices cooled with a liquid such as helium or nitrogen. When this cooling method is used, the amplifier structure (for example, a parametric amplifier) is partially or completely immersed in the coolant, although the coolant is usually kept out of spaces with electromagnetic fields. However, the active elements (such as varactor diodes or tunnel diodes) are located in the coolant-free space. The loss resistances of the active elements exhibit heat which in parametric amplifiers is due to ac pumping and in tunnel diodes is due to dc operation. This heat increases the ambient temperature of the lossy element and diminishes the noise-reduction effect of the coolant.

This reaction has been noticed in monostatic high-power radar systems which use parametric amplifiers as preamplifiers. Because of the leakage power, the varactor diodes used have a medium or low quality factor

$$Q_o = \frac{1}{2\pi f_c C_o R} \tag{1}$$

where

f_c cutoff frequency

C_o bias capacitance

R loss resistance

The leakage power together with the pump power generates heat in the lossy section of the diode so that increases in ambient temperature of 100^o to 150^o K are common. These increases are due to low heat conduction in the internal construction of varactor diodes. In order to eliminate this heat rise, an obvious answer is the use of liquid nitrogen as a coolant both inside and outside waveguides and cavity resonators of the parametric amplifier. This method was found to be successful in keeping the active element cool. However, for a variable-capacitance diode, bubble formation developed, especially in the neighborhood of the active element. This bubble formation causes the resonant frequency of the tuned circuit to change erratically because of the difference in the dielectric constants of liquid and gaseous states of the coolant. For example, the ratio of the dielectric constants of liquid to gaseous nitrogen is 1.435:1. (See ref. 1, p. 7.004.) In order to keep the heat source from creating gaseous nitrogen, pressurization was considered.

This report discusses procedures which can be used to determine the temperature rise and pressure requirements necessary to maintain nitrogen in liquid form within the cavity containing the heating element. Two methods, a theoretical procedure based on the heat-flow equations and an experimental procedure based on a salt-solution test, were applied to a typical 1-GHz cavity. These results were compared with the measurements made with a cavity which contained a resistor to simulate the lossy diode. In addition, this report treats the procedure for estimating the resonant frequency of the liquid-filled cavity and compares it to the measured value.

The author wishes to thank Prof. Dr.-Ing. Habil. Kurt Lamberts, Associate Professor of Technische Hochschule, Braunschweig, West Germany, for valuable discussion on the investigation methods.

SYMBOLS

a average length of flow lines within one sector, centimeters

A cross-sectional area of heat-flow penetration along the heat source, $b\ell$, centimeters^2

b	breadth of a sector, centimeters
B^*	equivalent side length, 0.44 centimeter
C	capacitance, farads
C_N	capacitance of cavity with liquid nitrogen, farads
C_o	bias capacitance, farads
C_r	capacitance of cavity at room temperature, farads
C_1, C_2, C_1^*, C_2^*	constants
d	distance of heat source from bottom of cavity, 0.5 centimeter
D	diameter of the heat source, 0.5 centimeter
f	frequency, hertz
Δf	bandwidth, hertz
f_c	cutoff frequency, hertz
f_N	resonant frequency of cavity with liquid nitrogen, hertz
f_r	resonant frequency of cavity at room temperature, hertz
$f(x)$	function of x given by equation (B10)
$g(x)$	function of x given by equation (B12)
$h(x)$	function of x given by equation (B7)
I	electric current, amperes
j	imaginary part

k	thermal conductivity, 1.4 milliwatts/centimeter-degree Kelvin
K	constant
l	length of the heat source, 1.5 centimeters
$l(x)$	function of x given by equation (B28)
L	inductance, henrys
m	number of isothermal lines (2 in present investigation)
n	number of heat-flow lines (12 in present investigation)
n(x)	function of x given by equation (B16)
p	pressure, atmospheres (1 atmosphere is equal to 101 kilonewtons/meter^2)
p(x)	function of x given by equation (B6)
q	thermal current density, watts/centimeter^2
q*	thermal current density of one sector, watts/centimeter^2
Q	heat flow, 50 milliwatts
Q*	heat flow for one sector, watts
Q_o	quality factor
Q_1	heat flow between surfaces S_1 and S_2, watts
Q_2	heat flow between surfaces S_3 and S_4, watts
Q_3	heat flow in the quadrants S_2-S_3, S_4-S_2, S_1-S_4, and S_3-S_1, watts
r,r*	radii of complex variables in polar coordinates
r_c	corner radius of the heat source (fig. 4), centimeters

$r(x)$	function of x given by equation (B20)
R	loss resistance, ohms
s	radial distance, centimeters
$s(x)$	function of x given by equation (B18)
S_1,S_2,S_3,S_4	dividing surfaces
$t(x)$	function of x given by equation (B4)
$t(y)$	function of y given in equation (B41)
T	temperature, degrees Kelvin
ΔT	temperature difference, degrees Kelvin
T_{oc}	temperature outside cavity, degrees Kelvin
T_s	temperature of heat source, degrees Kelvin
u,u^*	complex functions of heat-flow lines
v,v^*	complex functions of isothermal lines
V	voltage, volts
w,w^*	complex variables
x,y,z	rectangular coordinate system
Δx	path length in direction of heat flow
z,z^*	complex variables
α	angle of complex variables in polar coordinates (see eq. (A4))
β	angle of complex variables in polar coordinates (see eq. (A8))

ϵ relative dielectric constant of gaseous nitrogen (1)

ϵ_N relative dielectric constant of liquid nitrogen (1.435)

κ specific electrical conductivity, 1.14 millimhos/centimeter

ξ length of the line source, centimeters

ρ factor, centimeters

φ potential, volts

Primed symbols denote differentiation with respect to x or y.

THEORETICAL CALCULATION OF THE TEMPERATURE DIFFERENCE BETWEEN A HEAT SOURCE AND THE WALL OF THE CAVITY

Heat transfer in cryogenic liquids (ref. 2, pp. 16-21) is a complicated process which is difficult to predict with the theoretically derived equations for high temperatures. The theoretical heat transfer by convection per unit area is many times larger than the actual measured heat transfer. In order to obtain preliminary information about the type of heat transfer involved, the bubble formation on the outside of the test cavity was observed. The fact that the location of maximum boiling (with 50 mW being dissipated by the simulated diode) was underneath the cavity bottom and along the cavity wall closest to the heat source indicated that the heat transfer by conduction dominated the heat transfer by convection. If convection had been substantial, the maximum boiling would have been over the cavity top above the heat source. Therefore, it is assumed that the temperature difference $T_S - T_{OC}$ between the heat source and the cavity wall of figure 1 is small and, thus, the thermodynamic characteristics are such that the effective heat conductivity is equal to the true thermal conductivity (i.e., the Nusselt number becomes unity (ref. 3, p. 321)). The problem is then concerned with three-dimensional steady-state heat conduction. The differential equation (ref. 3, p. 109)

$$\frac{\partial^2 T}{\partial x^2} + \frac{\partial^2 T}{\partial y^2} + \frac{\partial^2 T}{\partial z^2} = 0 \tag{2}$$

describes the temperature distribution associated with the heat flow. This differential equation is similar to the potential equation for a stationary electric field (ref. 4, p. 117) given as

$$\frac{\partial^2 \varphi}{\partial x^2} + \frac{\partial^2 \varphi}{\partial y^2} + \frac{\partial^2 \varphi}{\partial z^2} = 0 \tag{3}$$

For both conditions, flow or displacement lines which are perpendicular to the isothermal or equipotential lines are involved. Hence, in calculating the temperature difference $T_s - T_{oc}$, the methods used in ascertaining field distribution in charge-free fields are applicable.

The application of this general method to a specific 1-GHz cavity is the most effective means of demonstrating the solution procedure. In order to study the conditions of

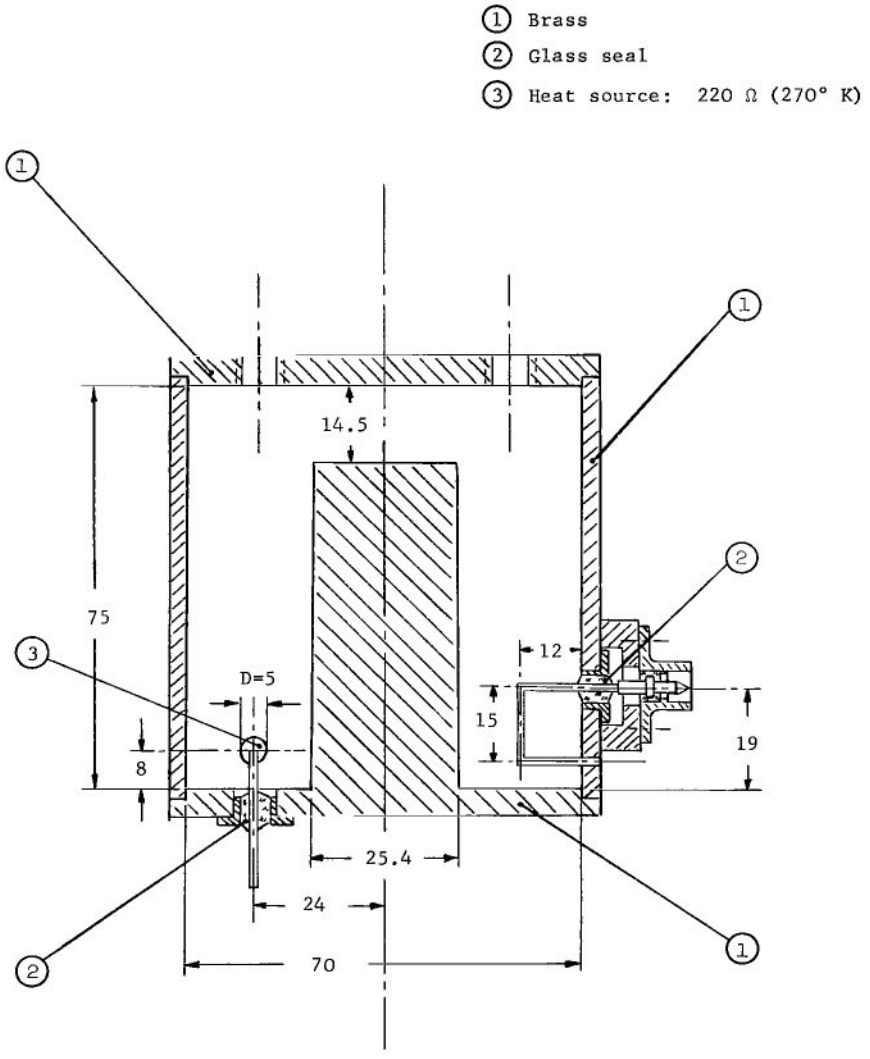

Figure 1.- Dimensions of the quarter-wavelength cavity for 1 GHz. All dimensions are in millimeters.

thermal conductivity for cooling with pressurized liquid nitrogen, the quarter-wavelength cavity resonator shown in figure 1 was designed in a coaxial arrangement. To allow pressurization, glass seals were used for the coupling loop and for the heat source. The heat source was located at the bottom of the cavity resonator in order to minimize the distortion in the electric field. However, the location of the active lossy element can be anywhere inside the cavity or waveguide depending on the kind of device and its purpose. The heat source was a 220-ohm resistor which was heated with direct current from the outside.

The leads for the liquid nitrogen are attached at two openings in the upper end of the cavity resonator. The cavity is immersed in liquid nitrogen at atmospheric pressure and the liquid nitrogen inside the cavity is pressurized. Under this condition the heat dissipated by boiling off liquid nitrogen takes place on the outer surface of the chamber under pressure (in this case, the cavity wall) instead of inside the cavity at the surface of the lossy element (heat source). A temperature gradient between the lossy element and the cavity wall builds up and the temperature of the lossy element increases.

The closed-form solution of a three-dimensional unsymmetric field (eq. (3)) is not available in the general case. In one method, the heat-flow field is simplified by dividing it into parts for which graphical and mathematical closed-form solutions are available. Figures 2(a) and 2(b) are sketches which show schematically how the heat-flow lines and isothermal lines run transversely and longitudinally through the cavity resonator. In simplifying the field, it is necessary to attempt to divide it into several partial fields which are easy to calculate. Figure 2(a) shows the division used with surfaces S_1 to S_4 perpendicular to the plane of the figure. The surfaces S_1 and S_2 limit the fairly homogeneous field in the longitudinal direction of the heat source. Edge effects at the ends of the heat source are calculated from the fields enclosed by surfaces S_3 and S_4 and from the quadrants enclosed by surfaces S_2 and S_3, S_4 and S_2, S_1 and S_4, and S_3 and S_1.

Heat Flow in the Field Between Surfaces S_1 and S_2

Because the length of the heat source is smaller than the diameter of the inner cylinder, the flow field is assumed to be essentially homogeneous in the longitudinal direction of the heat source. The calculation is thereby reduced to two dimensions. Because of the unequal spacing of the heat source from the walls of the cavity resonator, graphical methods as described in reference 4, pages 137-139, should be applied to the conditions of figure 2(c).

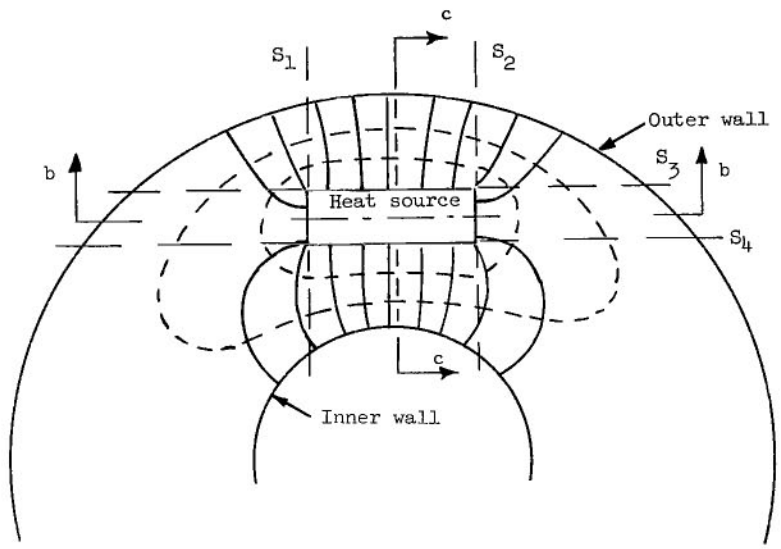

(a) Horizontal section of the cavity.

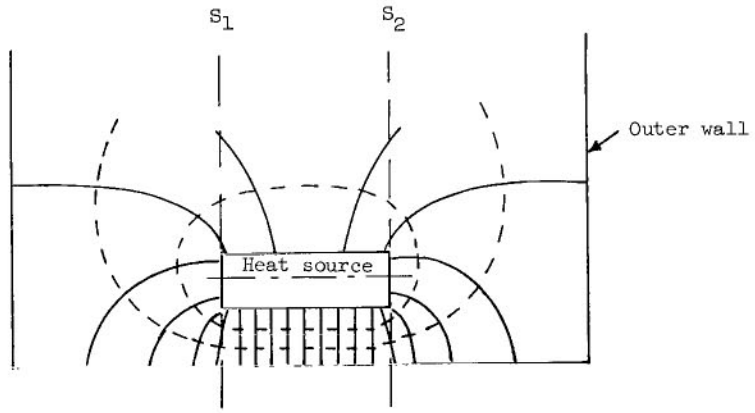

(b) Vertical section b-b of the cavity through the center line of the heat source.

Figure 2.- Heat flow and isothermal lines around the heat source.

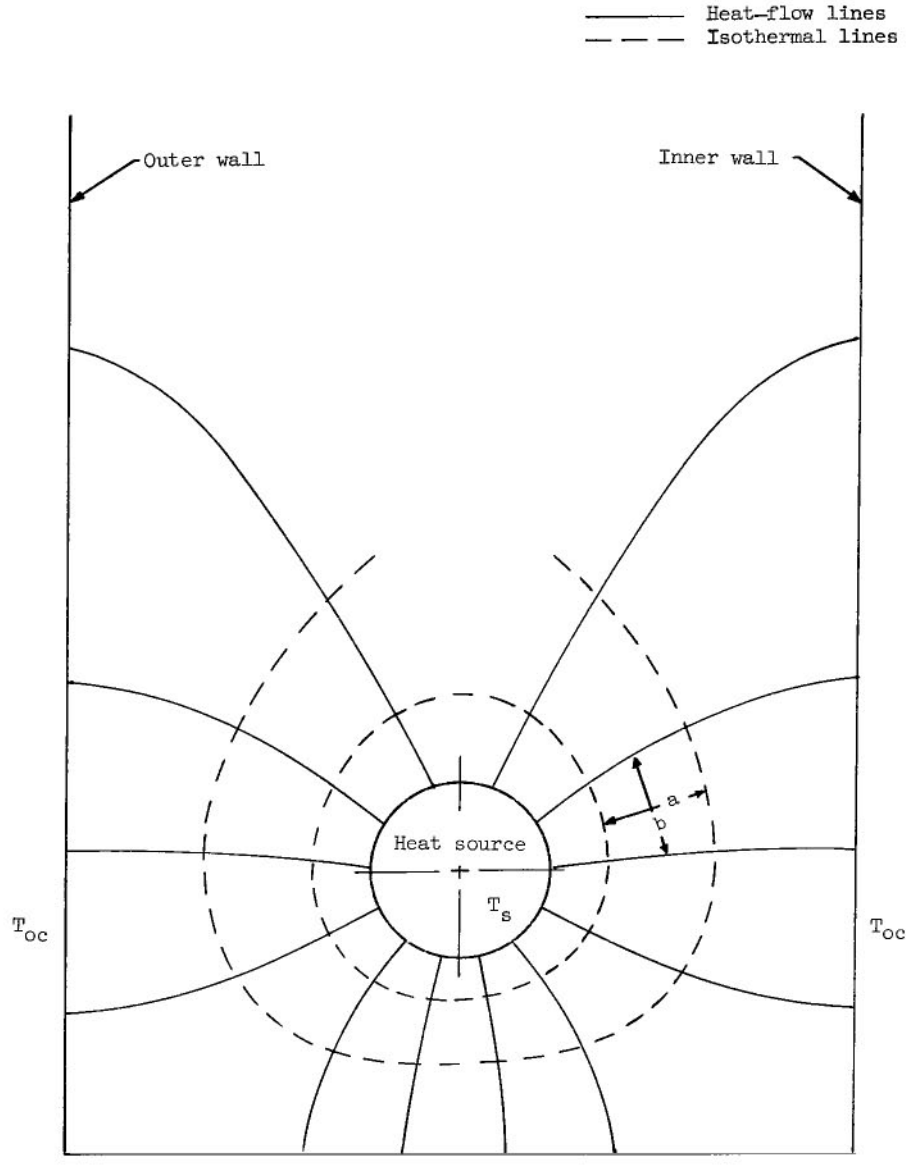

(c) Vertical section c-c through the heat source.

Figure 2.- Concluded.

The thermal current density is

$$q = -k\frac{\Delta T}{\Delta x} \tag{4}$$

where

k	thermal conductivity
ΔT	temperature difference
Δx	path length in the direction of heat flow

The negative sign indicates that heat flows with decreasing temperature. If applied to one sector of figure 2(c), the thermal current density becomes

$$q^* = -k\frac{\Delta T}{a} \tag{5}$$

where ΔT is the temperature difference between two neighboring isothermal lines and a is the average length of flow lines within one sector.

The thermal current density for the temperature difference $T_s - T_{oc}$ for the isothermal lines ($m = 2$ in fig. 2(c)) is then

$$q = k\frac{T_s - T_{oc}}{a(m + 1)} \tag{6}$$

The heat flow for one sector is

$$Q^* = qA \tag{7}$$

where $A = b\ell$ is the cross-sectional area of heat-flow penetration along the heat source. Combining equations (6) and (7) gives

$$Q^* = k\frac{T_s - T_{oc}}{(m + 1)}\frac{b}{a}\ell \tag{8}$$

The ratio $\frac{a}{b}$ is the scale factor which determines the shape but not the size of each sector. For $\frac{a}{b} = 1$, a square is approximated. The approximation to a square increases with the number of heat-flow lines and isothermal lines selected.

The total heat flow Q_1 for n heat-flow lines is

$$Q_1 = k(T_s - T_{oc})\, l\, \frac{b}{a}\, \frac{n}{m+1} \tag{9}$$

By using $\frac{b}{a} = 1$, $n = 1$, $n = 12$, $m = 2$, and $l = 1.5$ cm, as obtained by this graphical method, equation (9) becomes

$$Q_1 = 6.0k(T_s - T_{oc}) \tag{10}$$

Heat Flow in the Field Between Surfaces S_3 and S_4

The heat flow in the volume between surfaces S_3 and S_4 of figure 2(a) is taken, for simplicity, to be homogeneous over the breadth of the front surfaces of the heat source (i.e., the flow lines do not intersect surfaces S_3 and S_4). In addition, in calculating this heat flow from the edge regions, the front surface of the heat source should be considered to be square. Equating the square surface area to the equivalent circular area gives the equivalent side length of

$$B^* = \sqrt{\frac{D^2}{4}\pi} \tag{11}$$

where D is the diameter of the heat source. In order to simplify the calculation, the following assumptions about the flow field are made: the effect of the cylindrical walls on the end surfaces of the heat source is neglected and the effect of the distortion of the flow lines from the elliptical shape on the upper boundary of the face is considered to be negligible. With these assumptions the simple boundary conditions of figure 3 are obtained.

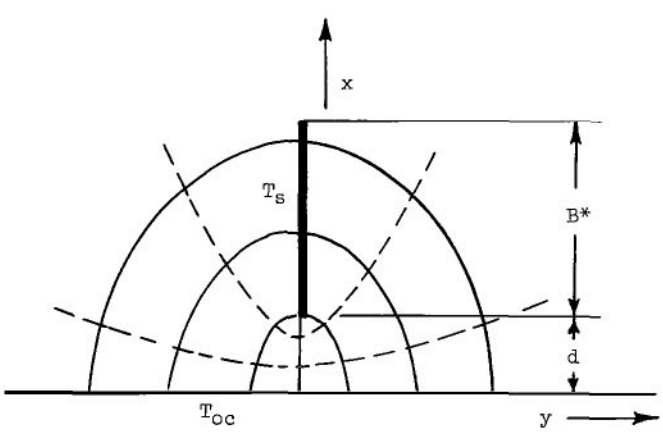

Figure 3.- Field line pattern on the front surfaces of the heat source.

The forms of the isothermal lines and flow lines are expected to be hyperbolic and elliptic, respectively. In order to satisfy the boundary conditions and solve the differential equation, the following equation as proposed by reference 4, pages 123-124, should be used:

$$w = u + jv = \cosh^{-1} z = \cosh^{-1}(x + jy) \tag{12}$$

In the special case of figure 3, constants must be introduced in order to satisfy the boundary conditions. Therefore, the following equation is applied:

$$w^* = u^* + jv^* = C_1 \cosh^{-1} Kz^* + C_2 \tag{13}$$

where C_1 and C_2 are, in general, complex numbers. By comparison with equation (12), the following relations are obtained:

$$z = Kz^* \tag{14}$$

and if $z = x + jy = 1 + j(0)$, then $z^* = d$. Hence, $K = \frac{1}{d}$, where d is the distance of the heat source from the bottom of the cavity as indicated in figure 3. In this calculation, the isothermal lines of the flow pattern of figure 3 are assigned to the v-curves and the following relations result:

$$w^* = C_1 w + C_2 \tag{15}$$

or

$$v^* = C_1^* v + C_2^* \tag{16}$$

The constants C_1 and C_2 are required to satisfy the boundary conditions. When $v = 0$, then $v^* = T_S$; when $v = -\frac{\pi}{2}$, then $v^* = T_{OC}$. After insertion of these values into equation (16), the constants are given as

$$C_1^* = \frac{2}{\pi}(T_S - T_{OC}) \tag{17}$$

$$C_2^* = T_S \tag{18}$$

The function for figure 3 may then be written

$$w^* = u^* + jv^* = \frac{2}{\pi}(T_S - T_{OC}) \cosh^{-1} \frac{1}{d}(x + jy) + T_S \tag{19}$$

The heat flow Q_2 in the volume between surfaces S_3 and S_4 can be calculated with the aid of the equation for the thermal current density given by

$$q = -k \operatorname{grad} T \tag{20}$$

where q and grad T are vectors. The gradient of the temperature T at the element surface is the partial derivative of the imaginary portion of equation (19) evaluated at $y = 0$ and is given by

$$\text{grad } T\Big|_{y=0} = \left|\frac{\partial \text{Im}(w^*)}{\partial x} + j\frac{\partial \text{Im}(w^*)}{\partial y}\right|_{y=0} \tag{21}$$

(Symbol Im signifies the imaginary part of eq. (19).)

The separation of the imaginary portion of the function of w^* is given in appendix A. The result is

$$v^* = C_1^* \tan^{-1} \frac{Ky + \sqrt[4]{K^4x^4 + K^4y^4 + 2K^4x^2y^2 - 2K^2x^2 + 2K^2y^2 + 1}\,\sin\dfrac{\tan^{-1}\dfrac{2K^2xy}{K^2x^2 - K^2y^2 - 1}}{2}}{Kx + \sqrt[4]{K^4x^4 + K^4y^4 + 2K^4x^2y^2 - 2K^2x^2 + 2K^2y^2 + 1}\,\cos\dfrac{\tan^{-1}\dfrac{2K^2xy}{K^2x^2 - K^2y^2 - 1}}{2}} + C_2^*$$

The partial derivative of this equation and the $y = 0$ restriction necessary to obtain the temperature gradient along the X-axis according to equation (21) is shown in detail in appendix B. The result is

$$\text{grad } T\Big|_{y=0} = C_1^* \frac{K + \dfrac{K^2x}{\sqrt{K^2x^2 - 1}}}{Kx + \sqrt{K^2x^2 - 1}} \tag{22}$$

By introducing the constants for the boundary conditions from equations (14), (17), and (18) and by combining them with equation (20), the thermal current density in the x-direction becomes

$$q = -k\frac{2}{\pi}\left(T_s - T_{oc}\right)\frac{\dfrac{1}{d} + \dfrac{\dfrac{1}{d^2}x}{\sqrt{\left(\dfrac{x}{d}\right)^2 - 1}}}{\dfrac{x}{d} + \sqrt{\left(\dfrac{x}{d}\right)^2 - 1}} \tag{23}$$

The heat flow Q_2 is calculated by integrating the thermal flow density over both sides of the front surface of the heat source as follows:

$$Q_2 = 2B^* \int_d^{d+B^*} q \, dx \tag{24}$$

Substituting equation (23) into equation (24) and carrying out the integration gives

$$Q_2 = \frac{4B^*k}{\pi}(T_s - T_{oc}) \ln \frac{d + B^* + \sqrt{B^*(2d + B^*)}}{d} \tag{25}$$

When $D = d = 0.5$ cm, equations (11) and (25) can be used to calculate Q_2 as

$$Q_2 = 0.7k(T_s - T_{oc}) \tag{26}$$

Heat Flow in the Field of Quadrants S_2-S_3, S_4-S_2, S_1-S_4, and S_3-S_1

The heat flow Q_3 is calculated for a perpendicular line source as shown in figure 4. The differential equation is

$$dT = Q \frac{d\xi}{B^* 4\pi k s} \tag{27}$$

where $d\xi$ is an infinitesimal section of the line source which contributes to the temperature rise at point P at the radial distance s. Solving equation (27) and rearranging it as presented in reference 4, pages 74-75 gives

$$Q_3 = k(T_s - T_{oc}) \frac{2\pi B^*}{\ln \frac{2B^*}{2r_c} \sqrt{\frac{4d + B^*}{4d + 3B^*}}} \tag{28}$$

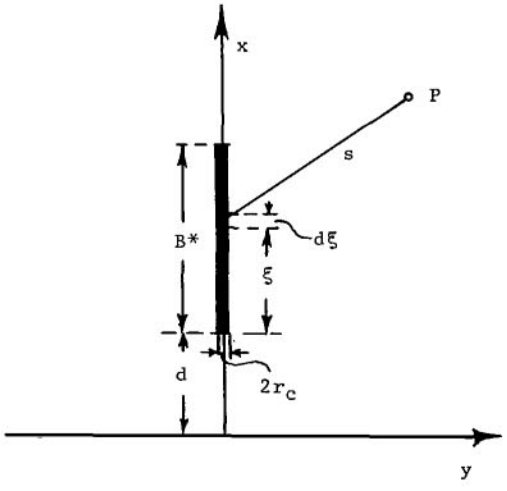

Figure 4.- Line source.

For $B^* = 0.44$ cm, $d = 0.5$ cm, and $2r_c = 0.1$ cm, the heat flow is

$$Q_3 = 1.4k(T_s - T_{oc}) \tag{29}$$

By summing equations (10), (26), and (29), the total heat flow from the heat source to the wall of the cavity is found to be

$$Q = 8.1k(T_s - T_{oc}) \tag{30}$$

The temperature rise due to the lossy element can be calculated from equation (30) as

$$T_s - T_{oc} = \frac{Q}{8.1k} \tag{31}$$

With the value $Q = 50$ mW (heat developed in the heat source), $T_{oc} = 77^{o}$ K (boiling temperature of the liquid nitrogen outside the cavity), and $k = 1.4$ mW/cm-^{o}K (thermal conductivity of liquid nitrogen at 77^{o} K (see ref. 1, p. 3.004)), the temperature of the heat source is calculated to be

$$T_s = 81.4^{o} \text{ K} \tag{32}$$

According to figure 5, which shows the pressure p of the liquid nitrogen as a function of the ambient temperature T at constant volume, the lowest pressure at which boiling will not take place for a temperature $T_s = 81.4^{o}$ K is $p = 1.6$ atm. Also see reference 1, page 6.004.

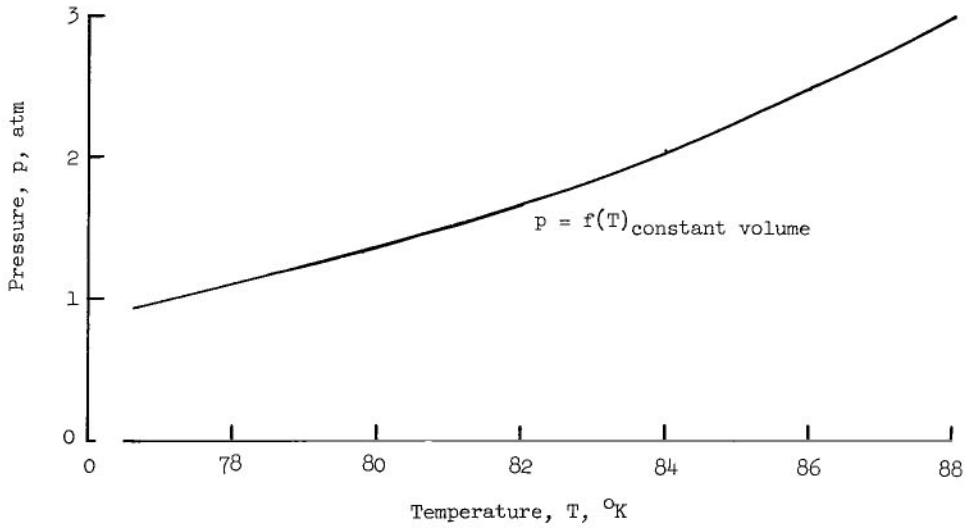

Figure 5.- Vapor pressure of liquid nitrogen as a function of temperature.

SALT-SOLUTION TEST

To test the results of equations (2) to (32), the following experiment, which is very similar to an investigation in an electrolytic tank, was carried out. As shown in figure 6,

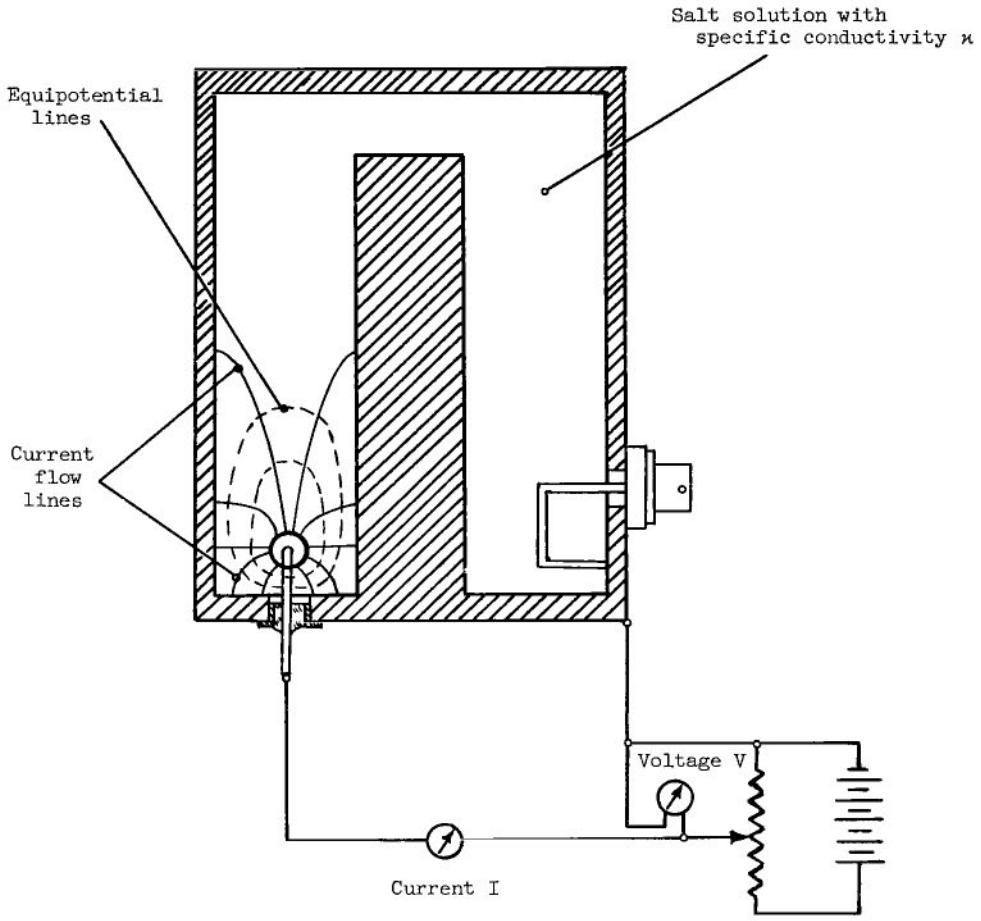

Figure 6.- Salt-solution-test setup.

the cavity was filled with a salt solution for which the specific conductivity (κ = 1.14 mmho/cm) was known. When a voltage V was applied between the electrode which had the shape of the heat source and the wall of the cavity, a current I commenced to pass through the salt solution. The side effect of heating the solution (negative temperature coefficient) and the side effect of the polarizing counter potential have to be minimized. The first can be controlled by using low voltages and low currents. The second can be overcome by using an ac generator or short current-flow times. When a 2-percent NaCl solution is used in the cavity of figure 6, a current-flow time of 3 seconds for 11 volts dc was short enough to keep the polarizing counter potential negligible.

The current I forms stream lines similar to heat-flow lines and equipotential lines similar to isothermal lines. Because the potential equations are identical, an electrical equation analogous to equation (31) can be written as

$$V = \frac{I}{\kappa\rho} \tag{33}$$

The factor ρ has the dimension of length and is given by the size, the shape, and the spacing of two opposing surfaces (for example, the number 8.1 in eq. (31)). Because V, I, and κ are known, ρ may be calculated. The measured and calculated values are

$$\left.\begin{aligned} V &= 11 \text{ volts} \\ I &= 150 \text{ mA} \\ \rho &= \frac{I}{V\kappa} = 12 \text{ cm} \end{aligned}\right\} \tag{34}$$

If the value of $\rho = 12$ cm is substituted into equation (31), the temperature of the heat source is given as

$$T_S = 80^{\circ} \text{ K} \tag{35}$$

The necessary pressure from figure 5 is 1.35 atm.

The temperature rise and the required pressure determined by the salt-solution test are smaller than those calculated by using equations (4) to (31). The reason for these differences is that assumptions were made for finding closed-form solutions of the field distribution. These assumptions have the effect that portions of some lines of the heat-flow field are lengthened. This lengthening increases the source temperature and the required pressure.

ESTIMATE OF THE RESONANT FREQUENCY OF THE LIQUID-FILLED CAVITY

In calculating the relative frequency change, the dimensions of the cavity are assumed to be effectively equal. The resonance frequency is

$$f = \frac{1}{2\pi\sqrt{LC}} \tag{36}$$

where L is the inductance of the cavity and C is the capacitance of the cavity. If the resonant frequency at room temperature is f_r and the resonant frequency with liquid

nitrogen in the cavity is f_N, the relative frequency change is

$$\frac{f_r - f_N}{f_r} = \frac{\Delta f}{f_r} = \left(\frac{1}{2\pi\sqrt{LC_r}} - \frac{1}{2\pi\sqrt{LC_N}}\right)2\pi\sqrt{LC_r} \tag{37}$$

or

$$\frac{\Delta f}{f_r} = 1 - \sqrt{\frac{C_r}{C_N}} \tag{38}$$

Under the previously mentioned conditions, the capacitances C_r and C_N of the cavity depend only on the relative dielectric constants. Therefore, the frequency change is

$$\frac{\Delta f}{f_r} = 1 - \sqrt{\frac{\epsilon}{\epsilon_N}} \tag{39}$$

where $\epsilon = 1$ is the relative dielectric constant of gaseous nitrogen and $\epsilon_N = 1.435$ is the relative dielectric constant of liquid nitrogen. (See ref. 1, p. 7.004.) Thus,

$$\frac{\Delta f}{f_r} = 0.165 \text{ or } 16.5 \text{ percent} \tag{40}$$

EXPERIMENTAL TESTS

The measurement setup shown in figure 7 was used to check the frequency stability of the cavity resonator during heat dissipation and to determine the resonant-frequency ratio of the empty to the liquid-nitrogen-filled cavity. This test method was selected because it was difficult to measure T_s directly and because the test would be extremely sensitive to the occurrence of nitrogen gas caused by boiling at the lossy element. The output power of the sweep generator was fed into the cavity, and the cavity output was connected to the detector. The resonance curve of the cavity was displayed on the face plate of the oscilloscope. Frequency markers in multiples of 1 MHz were displayed simultaneously with the resonance curve by means of frequency-marker generators and a capacitive coupler. A dc source delivered the power for the heat source.

Changes in the dielectric constant caused by boiling within the cavity resonator were revealed by the trace as a shift of the resonance point in the horizontal direction. It was then possible to determine shifts of the resonance point to a fraction of 1 MHz.

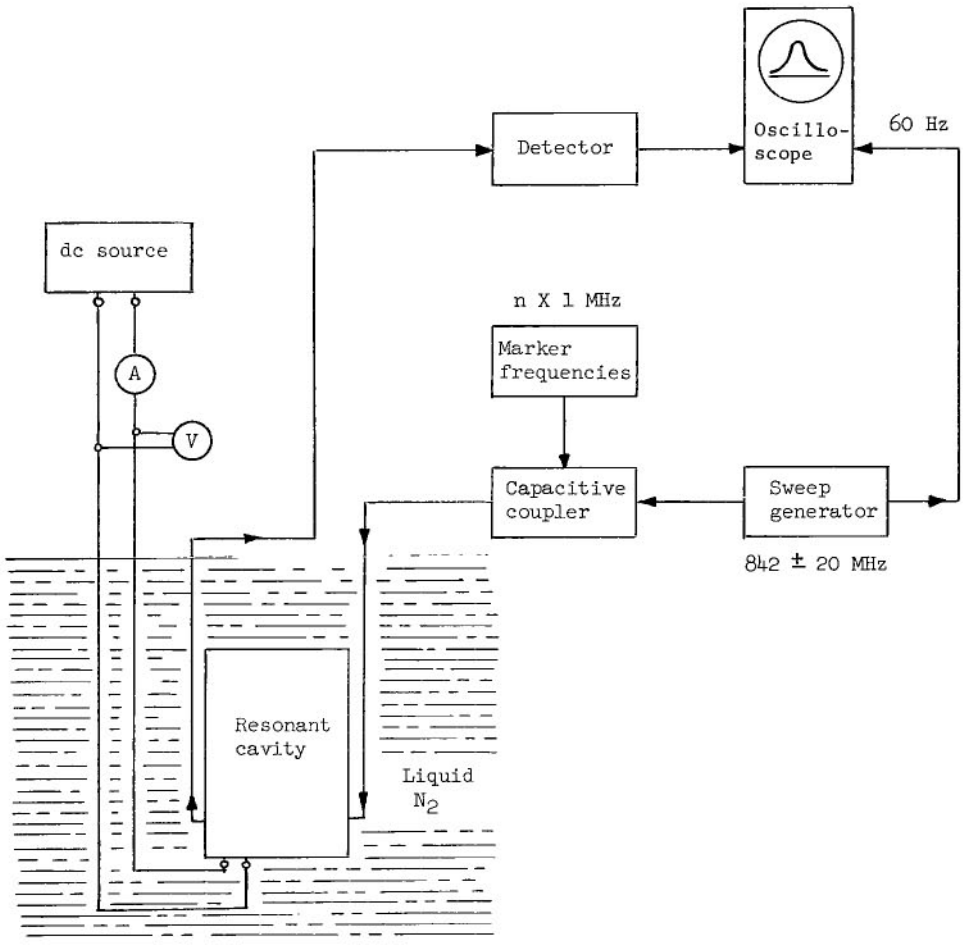

Figure 7.- Measurement of the frequency stability of the resonant cavity filled with liquid nitrogen.

RESULTS

This investigation revealed that when the heat flow was 50 mW, the pressure inside the cavity had to be raised to 1.4 atm to prevent a shift of the resonance point at the oscilloscope. The following table lists the results of the theoretical method, the salt-solution test, and the measurement:

Method	Temperature rise, ^{o}K	Pressure, atm
Theoretical calculation	4.4	1.6
Salt-solution test	3	1.35
Measurement	3.3	1.4

The results of the salt-solution test and of the measurement agree well. The theoretical investigation is also in very good agreement considering the approximations used for calculating the heat flow in the asymmetrical fields.

The measured resonant frequencies are

$$f_r = 1003.18 \text{ MHz}$$

$$f_N = 841.85 \text{ MHz}$$

and give

$$\frac{\Delta f}{f_r} = 0.161 \text{ or } 16.1 \text{ percent}$$

Because the agreement between calculated and measured frequency change due to the transition from gaseous state to liquid state is sufficient, the amplifier may be designed directly for operation with liquid coolant in the cavity.

This cooling with pressurized liquid nitrogen has been used successfully in prototype parametric amplifiers with medium-quality varactor diodes in radar installations. The entire amplifier including signal circuit, idler circuit, and pump coupling was inserted into a pressure container with openings throughout the cavities so that every unit, including the diode housing, was in contact with the pressurized liquid nitrogen. The measured input-noise temperature of this amplifier was within $\pm 5^{o}$ K of the calculated value when a noise-measuring system with an accuracy of $\pm 3^{o}$ K was used. The accuracy was achieved with hot- and cold-body standard noise sources. The investigations also

revealed that the overloading power limit of the varactor diode due to leakage power in radar systems was increased by a factor of 100.

With a heat flow of 5 watts, a pressure of only 1.6 atm was necessary to suppress resonant-frequency changes. This condition indicates that convection in addition to stationary heat conduction becomes significant at higher heat flows and, thus, empirical equations as given in reference 3, pages 298-323, must be applied.

CONCLUDING REMARKS

The temperature rise in lossy capacitance diodes in cooled parametric amplifiers is a problem. It has been established that the use of pressurized liquid coolant inside cavities such as resonators, waveguides, and diode cavities is an effective method for suppression of the temperature rise. Investigation has been conducted in detail on 1-GHz coaxial cavity. Two methods for the determination of the temperature rise at the diode have been developed for the 1-GHz coaxial cavity as follows: (a) calculation with an assumption that reduces the heat-flow field to mathematical closed-form solutions and (b) application of a salt-solution test. In the theoretical determination of the temperature rise, a form factor ρ of unit length was obtained which takes into account essentially the shape, the size, and the distance of the two opposite heat potential surfaces. It has been demonstrated that this factor ρ can also be determined with the salt-solution test. The calculation yielded a temperature-rise estimate of 4.4° K and the salt-solution test, an estimate of 3° K. Because the simplification necessary for the calculation of the heat-flow field led to a partial lengthening of some streamlines, some difference can be expected. Therefore, the salt-solution test is a simple and fast measuring method for the determination of the temperature rise of lossy diodes and may replace tedious and lengthy calculations.

Measurements of the temperature rise in a test cavity at 1 GHz were obtained for comparison with the preceding methods. The pressure required to suppress bubble formation has been measured and a corresponding temperature rise of 3.3° K above the temperature of liquid nitrogen at 1 atmosphere has been obtained. This result is in good agreement with the salt-solution test. Finally, the determination of the resonant-frequency change for the use of liquid nitrogen within the cavity has shown that the measured values deviate by only 0.4 percent from the calculated ones.

Langley Research Center,
National Aeronautics and Space Administration,
Langley Station, Hampton, Va., December 19, 1967,
125-22-03-02-23.

APPENDIX A

SEPARATION OF THE IMAGINARY PORTION OF THE FUNCTION w^*

The function of equation (13)

$$w^* = u^* + jv^* = C_2 + C_1 \cosh^{-1} K(x + jy) \tag{A1}$$

can be written in the identical logarithmic form as

$$u^* + jv^* = C_2 + C_1 \ln\left[K(x + jy) + \sqrt{K^2(x + jy)^2 - 1}\right] \tag{A2}$$

By applying the polar-coordinate notation for the complex variables, equation (A2) becomes

$$u^* + jv^* = C_2 + C_1 \ln\left[K(x + jy) + \sqrt{re^{j\alpha}}\right] \tag{A3}$$

where

$$\alpha = \tan^{-1} \frac{2K^2xy}{K^2x^2 - K^2y^2 - 1} \tag{A4}$$

and

$$r = \left[\left(K^2x^2 - K^2y^2 - 1\right)^2 + 4K^4x^2y^2\right]^{1/2} \tag{A5}$$

Solving the square root, using de Moivre's relation for complex variables, and rearranging yields

$$u^* + jv^* = C_2 + C_1 \ln\left[Kx + \sqrt{r} \cos\frac{\alpha}{2} + j\left(Ky + \sqrt{r} \sin\frac{\alpha}{2}\right)\right] \tag{A6}$$

By using the polar-coordinate notation again, equation (A6) is simplified to

$$u^* + jv^* = C_2 + C_1 \ln r^* e^{j\beta} \tag{A7}$$

where

$$\beta = \tan^{-1} \frac{Ky + \sqrt{r} \sin\frac{\alpha}{2}}{Kx + \sqrt{r} \cos\frac{\alpha}{2}} \tag{A8}$$

and

$$r^* = \left[\left(Kx + \sqrt{r}\cos\frac{\alpha}{2}\right)^2 + \left(Ky + \sqrt{r}\sin\frac{\alpha}{2}\right)^2\right]^{1/2} \tag{A9}$$

Taking the log in equation (A7), which is the final step for the separation of the real from the imaginary portion of equation (A1), yields

$$u^* + jv^* = C_2 + C_1 \ln r^* + jC_1\beta \tag{A10}$$

The imaginary part is

$$v^* = C_1^*\beta + C_2^* \tag{A11}$$

or, after insertion of equations (A8), (A5), and (A4) into equation (A11), the expression for v^* becomes

$$v^* = C_1^* \tan^{-1} \frac{Ky + \sqrt[4]{K^4x^4 + K^4y^4 + 2K^4x^2y^2 - 2K^2x^2 + 2K^2y^2 + 1}\,\sin\dfrac{\tan^{-1}\dfrac{2K^2xy}{K^2x^2 - K^2y^2 - 1}}{2}}{Kx + \sqrt[4]{K^4x^4 + K^4y^4 + 2K^4x^2y^2 - 2K^2x^2 + 2K^2y^2 + 1}\,\cos\dfrac{\tan^{-1}\dfrac{2K^2xy}{K^2x^2 - K^2y^2 - 1}}{2}} + C_2^* \tag{A12}$$

APPENDIX B

PARTIAL DERIVATIVE AND $y = 0$ RESTRICTION OF EQUATION (A12)

The sequence of operations performed on equation (A12) must be observed. However, the $y = 0$ restriction can be applied immediately after taking the derivative of any factor of equation (A12) without changing the meaning. This procedure will simplify the calculation. Equation (A12) repeated here for convenience as (B1) is

$$v^* = C_1^* \tan^{-1} \frac{Ky + \sqrt[4]{K^4x^4 + K^4y^4 + 2K^4x^2y^2 - 2K^2x^2 + 2K^2y^2 + 1}\, \sin \frac{\tan^{-1} \dfrac{2K^2xy}{K^2x^2 - K^2y^2 - 1}}{2}}{Kx + \sqrt[4]{K^4x^4 + K^4y^4 + 2K^4x^2y^2 - 2K^2x^2 + 2K^2y^2 + 1}\, \cos \dfrac{\tan^{-1} \dfrac{2K^2xy}{K^2x^2 - K^2y^2 - 1}}{2}} + C_2^* \tag{B1}$$

The argument of the $\tan^{-1}$ will be called $t(x)$. Equation (B1) can then be written as

$$v^* = C_1^* \tan^{-1} t(x) + C_2^* \tag{B2}$$

and the derivative of the first term of the partial differentiation is then

$$\frac{\partial v^*}{\partial x} = C_1^* \frac{1}{1 + t(x)^2} t'(x) \tag{B3}$$

The function $t(x)$ represents

$$t(x) = \frac{h(x)}{p(x)} \tag{B4}$$

Differentiation of the quotient gives

$$t'(x) = \frac{h'(x)p(x) - h(x)p'(x)}{p(x)^2} \tag{B5}$$

where $h(x)$ and $p(x)$ are

$$p(x) = Kx + f(x)g(x) \tag{B6}$$

$$h(x) = Ky + f(x)\ell(x) \tag{B7}$$

To obtain $p'(x)$ and $h'(x)$, the differentiations of the sum and the product are used as follows:

$$p'(x) = K + f'(x)g(x) + f(x)g'(x) \tag{B8}$$

$$h'(x) = f'(x)\ell(x) + f(x)\ell'(x) \tag{B9}$$

where

$$f(x) = \sqrt[4]{K^4x^4 + K^4y^4 + 2K^4x^2y^2 - 2K^2x^2 + 2K^2y^2 + 1} \tag{B10}$$

$$f'(x) = \frac{1}{4}\frac{4K^4x^3 + 4K^4xy^2 - 4K^2x}{\left(K^4x^4 + K^4y^4 + 2K^4x^2y^2 - 2K^2x^2 + 2K^2y^2 + 1\right)^{3/4}} \tag{B11}$$

$$g(x) = \cos\frac{1}{2}n(x) \tag{B12}$$

$$g'(x) = -\frac{1}{2}\left[\sin\frac{1}{2}n(x)\right]n'(x) \tag{B13}$$

The functions $\ell(x)$ and $\ell'(x)$ will be defined subsequently.

For $y = 0$, equations (B10) and (B11) become

$$f(x)\big|_{y=0} = \pm\sqrt{K^2x^2 - 1} \tag{B14}$$

$$f'(x)\big|_{y=0} = \frac{K^2x}{\pm\sqrt{K^2x - 1}} \tag{B15}$$

The function $n(x)$ represents the $\tan^{-1}$ of the numerator and denominator of equation (B1) and is given by

$$n(x) = \tan^{-1}\frac{s(x)}{r(x)} \tag{B16}$$

The derivative is

$$n'(x) = \frac{1}{1 + \left[\frac{s(x)}{r(x)}\right]^2} \frac{s'(x)r(x) - s(x)r'(x)}{r(x)^2} \tag{B17}$$

where

$$s(x) = 2K^2xy \tag{B18}$$

$$s'(x) = 2K^2y \tag{B19}$$

$$r(x) = K^2x^2 - K^2y^2 - 1 \tag{B20}$$

$$r'(x) = 2K^2x \tag{B21}$$

Setting $y = 0$ results in

$$s(x)\big|_{y=0} = 0 \tag{B22}$$

$$s'(x)\big|_{y=0} = 0 \tag{B23}$$

$$r(x)\big|_{y=0} = K^2x^2 - 1 \tag{B24}$$

$$r'(x)\big|_{y=0} = 2K^2x \tag{B25}$$

When equations (B22), (B23), (B24), and (B25) are inserted into equation (B17), the condition for $y = 0$ for the function $n'(x)$ is

$$n'(x)\big|_{y=0} = 0 \tag{B26}$$

and equations (B24) and (B18) applied to equation (B16) result in

$$n(x)\big|_{y=0} = 0 \tag{B27}$$

The function $\ell(x)$ represents the sine in the numerator of equation (B1) and is given by

$$\ell(x) = \sin \frac{1}{2} n(x) \tag{B28}$$

and the derivative is

$$l'(x) = \frac{1}{2}\left[\cos \frac{1}{2} n(x)\right] n'(x) \tag{B29}$$

The results of equations (B26) and (B27) inserted into equations (B12), (B13), (B28), and (B29) give

$$g(x)\big|_{y=0} = 1 \tag{B30}$$

$$g'(x)\big|_{y=0} = 0 \tag{B31}$$

$$l(x)\big|_{y=0} = 0 \tag{B32}$$

$$l'(x)\big|_{y=0} = 0 \tag{B33}$$

Equations (B30), (B31), (B32), (B33), (B14), and (B15) applied to equations (B6), (B7), (B8), and (B9) give the following results:

$$p(x)\big|_{y=0} = Kx + \sqrt{K^2x^2 - 1} \tag{B34}$$

$$h(x)\big|_{y=0} = 0 \tag{B35}$$

$$p'(x)\big|_{y=0} = K + \frac{2K^2x}{\sqrt{K^2x^2 - 1}} \tag{B36}$$

$$h'(x)\big|_{y=0} = 0 \tag{B37}$$

Equations (B34) to (B37) inserted into equations (B4) and (B5) give

$$t(x)\big|_{y=0} = 0 \tag{B38}$$

$$t'(x)\big|_{y=0} = 0 \tag{B39}$$

and the insertion of these results into equation (B3) shows that

$$\left.\frac{\partial v^*}{\partial x}\right|_{y=0} = 0 \tag{B40}$$

The same procedure has to be applied for the computation of the second term of the partial derivative

$$\frac{\partial v^*}{\partial y} = C_1^* \frac{1}{1 + t^2(y)} t'(y) \tag{B41}$$

where the function $t(y)$ is the argument of the first $\tan^{-1}$ of equation (B1) with the variable y. By using the same differentiation rules and substitution methods shown in equations (B4) to (B39), with respect to y, the result becomes

$$\frac{\partial v^*}{\partial y} = jC_1^* \frac{K + \dfrac{K^2 x}{\sqrt{K^2 x^2 - 1}}}{Kx + \sqrt{K^2 x^2 - 1}} \tag{B42}$$

The j-factor indicates only that the gradient of the temperature at the location $y = 0$ is perpendicular to the face plane of the heating element.

REFERENCES

1. Johnson, Victor J., ed.: A Compendium of the Properties of Materials at Low Temperature (Phase I). Part I. Properties of Fluids. WADD Tech. Rept. 60-56, Pt. I, U.S. Air Force, Oct. 1960.

2. Richards, R. J.; Steward, W. G.; and Jacobs, R. B.: A Survey of the Literature on Heat Transfer From Solid Surfaces to Cryogenic Fluids. NBS Tech. Note No. 122 (PB 161623), U.S. Dep. Com., Oct. 1961.

3. Gröber, H.; and Erk, S. (Jerzy R. Moszynski, trans.): Fundamentals of Heat Transfer. McGraw-Hill Book Co., Inc., 1961.

4. Küpfmüller, Karl: Einführung in die theoretische Elektrotechnik. Springer Verlag (Berlin), 1952.

NASA-Langley, 1968 — 9 L-5536